Cancer Cell
Article

Integrative Analysis Reveals an Outcome-Associated and Targetable Pattern of p53 and Cell Cycle Deregulation in Diffuse Large B Cell Lymphoma

Stefano Monti,[1,8,9] Bjoern Chapuy,[2,8] Kunihiko Takeyama,[2,10] Scott J. Rodig,[5] Yansheng Hao,[2] Kelly T. Yeda,[2] Haig Inguilizian,[4] Craig Mermel,[1] Treeve Currie,[5,11] Ahmet Dogan,[6] Jeffery L. Kutok,[5,12] Rameen Beroukhim,[1] Donna Neuberg,[3] Thomas M. Habermann,[7] Gad Getz,[1] Andrew L. Kung,[4] Todd R. Golub,[1,4] and Margaret A. Shipp[2,*]
[1]Cancer Program, Broad Institute, Cambridge, MA 02142, USA
[2]Department of Medical Oncology
[3]Department of Biostatistics
[4]Department of Pediatric Oncology
Dana-Farber Cancer Institute, Boston, MA 02215, USA
[5]Department of Pathology, Brigham and Women's Hospital, Boston, MA 02115, USA
[6]Department of Laboratory Medicine and Pathology, College of Medicine
[7]Division of Hematology
Mayo Clinic, Rochester, MN 55905, USA
[8]These authors contributed equally to this work
[9]Present address: Section of Computational Biomedicine, Boston University School of Medicine, Boston, MA 02118, USA
[10]Present address: Sanofi-Aventis K. K., 163-1488 Tokyo, Japan
[11]Present address: Novartis, Cambridge, MA 02139, USA
[12]Present address: Infinity Pharmaceuticals, Cambridge, MA 02139, USA
*Correspondence: margaret_shipp@dfci.harvard.edu
http://dx.doi.org/10.1016/j.ccr.2012.07.014

SUMMARY

Diffuse large B cell lymphoma (DLBCL) is a clinically and biologically heterogeneous disease with a high proliferation rate. By integrating copy number data with transcriptional profiles and performing pathway analysis in primary DLBCLs, we identified a comprehensive set of copy number alterations (CNAs) that decreased p53 activity and perturbed cell cycle regulation. Primary tumors either had multiple complementary alterations of p53 and cell cycle components or largely lacked these lesions. DLBCLs with p53 and cell cycle pathway CNAs had decreased abundance of p53 target transcripts and increased expression of E2F target genes and the Ki67 proliferation marker. CNAs of the CDKN2A-TP53-RB-E2F axis provide a structural basis for increased proliferation in DLBCL, predict outcome with current therapy, and suggest targeted treatment approaches.

INTRODUCTION

Diffuse large B cell lymphoma (DLBCL) is the most common non-Hodgkin lymphoma in adults and a clinically and genetically heterogeneous disorder. With current immunochemotherapy, over 60% of patients with DLBCL can be cured; however, the remaining patients succumb to their disease (Friedberg and Fisher, 2008). Despite recent advances in the molecular understanding of DLBCL pathogenesis, clinical risk factor models are still used to identify patients who are unlikely to be cured with current therapy. The most widely used model is the International Prognostic Index (IPI), an outcome predictor based on easily measurable clinical parameters including age, performance status, serum lactate dehydrogenase (LDH), Ann Arbor stage, and number of extranodal disease sites (Shipp et al., 1993). Although the IPI is robust and reproducible, the link between the included

Significance

In spite of advances in the molecular understanding of DLBCL pathogenesis, clinical models are still used to identify high-risk patients who then receive empiric therapy. In DLBCLs, which have infrequent inactivating somatic mutations of *TP53* and *RB1*, the current studies define an alternative copy number-dependent mechanism of deregulating p53 and cell cycle. This genetic signature predicts outcome and suggests targeted approaches to treatment such as pan cyclin-dependent kinase inhibition.

clinical parameters and underlying biology or targeted treatment remains to be defined.

In previous studies, increased cellular proliferation has also been associated with unfavorable outcome in DLBCL. Indirect indices of cellular proliferation included elevated serum LDH as a component of the IPI and increased expression of the Ki67 nuclear antigen (Grogan et al., 1988; Salles et al., 2011).

DLBCLs largely originate from germinal center (GC) B cells, which have high growth rates and increased genomic instability (Klein and Dalla-Favera, 2008). GC B cells undergo somatic hypermutation (SHM) of their immunoglobulin variable region genes and class-switch recombination (CSR) to alter their immunoglobulin subtype. The rapid proliferation rate and errors in CSR and SHM predispose normal GC B cells to malignant transformation. As a consequence, DLBCLs exhibit multiple low frequency genetic alterations including chromosomal translocations, somatic mutations, and copy number alterations (CNAs).

Given the numbers and types of genetic alterations in DLBCL, investigators have sought additional comprehensive classification systems to identify groups of tumors with similar molecular traits. Transcriptional profiling has been used to define DLBCL subsets that share certain features with normal B cell subtypes (''cell-of-origin'' [COO] classification) (Lenz and Staudt, 2010). COO-defined DLBCLs include ''germinal center B cell'' (GCB) and ''activated B cell'' (ABC) types and an additional group of unclassified tumors. The COO-defined tumor groups are characterized by certain biological features, most notably increased NFκB activity and less favorable outcome in ABC-type DLBCLs (Lenz and Staudt, 2010). However, the outcome differences in GCB and ABC-type DLBCLs may be less striking in patients treated with current rituxan-containing combination chemotherapy regimens (Fu et al., 2008; Lenz et al., 2008a). An alternative transcriptional profiling classification, termed comprehensive consensus clustering, identifies DLBCL subtypes solely on the basis of distinctions within primary tumors and includes the three groups: ''B cell receptor,'' ''oxidative phosphorylation,'' and ''host-response'' (Chen et al., 2008; Monti et al., 2005).

To date, genetic alterations in DLBCL have largely been analyzed as single features or in association with the defined transcriptional subtypes (Bea et al., 2005; Lenz et al., 2008b). The platforms that were previously used to define CNAs in DLBCL had lower resolution, and concordant assessments of transcript abundance and copy number (CN) were more limited. For these reasons, the precise boundaries of CNAs, the associated candidate ''driver genes,'' and implicated pathways require further definition.

The earlier observations regarding cellular proliferation in DLBCL prompted additional analyses of certain individual cell cycle components and regulators. Cell cycle progression is controlled by series of cyclin-dependent kinases (CDKs), which are complexed with specific cyclins (Malumbres and Barbacid, 2009). The cyclin D-dependent kinases 4 and 6 (CDK4/CDK6) and the cyclin E-associated kinase 2 (CDK2) sequentially phosphorylate the retinoblastoma (RB) proteins, releasing the E2F transcription factors and promoting cell cycle progression. The A-type cyclins also activate CDK2 and CDK1 promoting S phase transition and the onset of mitosis. CDK activity is regulated by inhibitors, such as the INK4 family member $p16^{INK4A}$ (at the *CDKN2A* locus), and certain p53 targets, such as p21, among others (Malumbres and Barbacid, 2009). Individual cell cycle components and regulators reported to be perturbed in small numbers of DLBCLs include *CDKN2A* (ARF and $p16^{INK4A}$), p53 and its target p21, cyclin D3, and RB1 (Jardin et al., 2010; Pasqualucci et al., 2011; Sánchez-Beato et al., 2003; Winter et al., 2010; Young et al., 2008). Recent deep sequencing analyses confirm earlier reports of *TP53* somatic mutations in approximately 20% of DLBCLs (Morin et al., 2011; Pasqualucci et al., 2011; Lohr et al., 2012), a much lower percentage than in certain nonhematologic malignancies (Cancer Genome Atlas Research Network, 2008, 2011). The relatively low frequency of *TP53* somatic alterations in primary human DLBCLs suggests that additional bases of p53 deficiency remain to be defined.

Herein, we integrate CN data with transcriptional profiles and perform pathway analyses to identify core deregulated and targetable pathways in primary DLBCLs.

RESULTS

Mapping Recurrent CNAs in Primary DLBCL

Recurrent CNAs in the 180 primary DLBCLs were detected using the Genomic Identification of Significant Targets in Cancer (GISTIC) algorithm. Within the identified regions of significant CN gain or loss, narrower peaks of maximally significant CN change were identified (Supplemental Experimental Procedures available online). We found 47 recurrent CNAs, including 21 copy gains and 26 copy losses, with frequencies of 4% to 27% (Figure 1; Table S1). The GISTIC-defined CNAs range from narrow focal alterations, such as amplification peak 2p16.1 to chromosome arm and whole-chromosome alterations, including gain of 1q, loss of 6q, and gain of chromosome 7 (Figure 1).

Comparison of CNAs in DLBCLs and Nonhematologic Cancers

To distinguish between CNAs that are unique to DLBCL and those that are found in other tumors, we compared the DLBCL GISTIC analysis to that of 2,433 nonhematologic cancers (Beroukhim et al., 2010). The CNAs in DLBCLs and the nonhematologic cancers were visualized with a mirror plot (Figure 2), and the CNA overlap in the two series was computed (Figure S1A; Supplemental Experimental Procedures). Seven of 21 (33%) regions of copy gain and 16/26 (62%) regions of copy loss were common to both series; additional regions of copy gain exhibited partial overlap (Figures 2 and S1A). Examples of shared alterations include gains of chromosome 7 and chromosome 1q and loss of chromosome 6q, suggesting a broader role for these alterations in multiple tumor types. In contrast, 9/21 (43%) regions of copy gain and 10/26 (38%) regions of copy loss were only identified in DLBCL, including gains of 2p16.1 and 19q13.42 (Figures 2 and S1A). These DLBCL-selective CNAs were largely absent in a lymphoid malignancy of non-GC origin (Figure S1B).

Integrative Analysis of CNAs and Transcript Abundance

We anticipated that DLBCL CNAs would alter the corresponding gene transcript levels and prioritized genes with the most significant association between transcript abundance and CNA. All genes within the 47 defined CNA peaks and regions (Table S2) were analyzed for the association between transcript abundance and the presence/absence of the gene alteration (peak or region) across the DLBCL series. The ''cis-signature'' of a given CNA

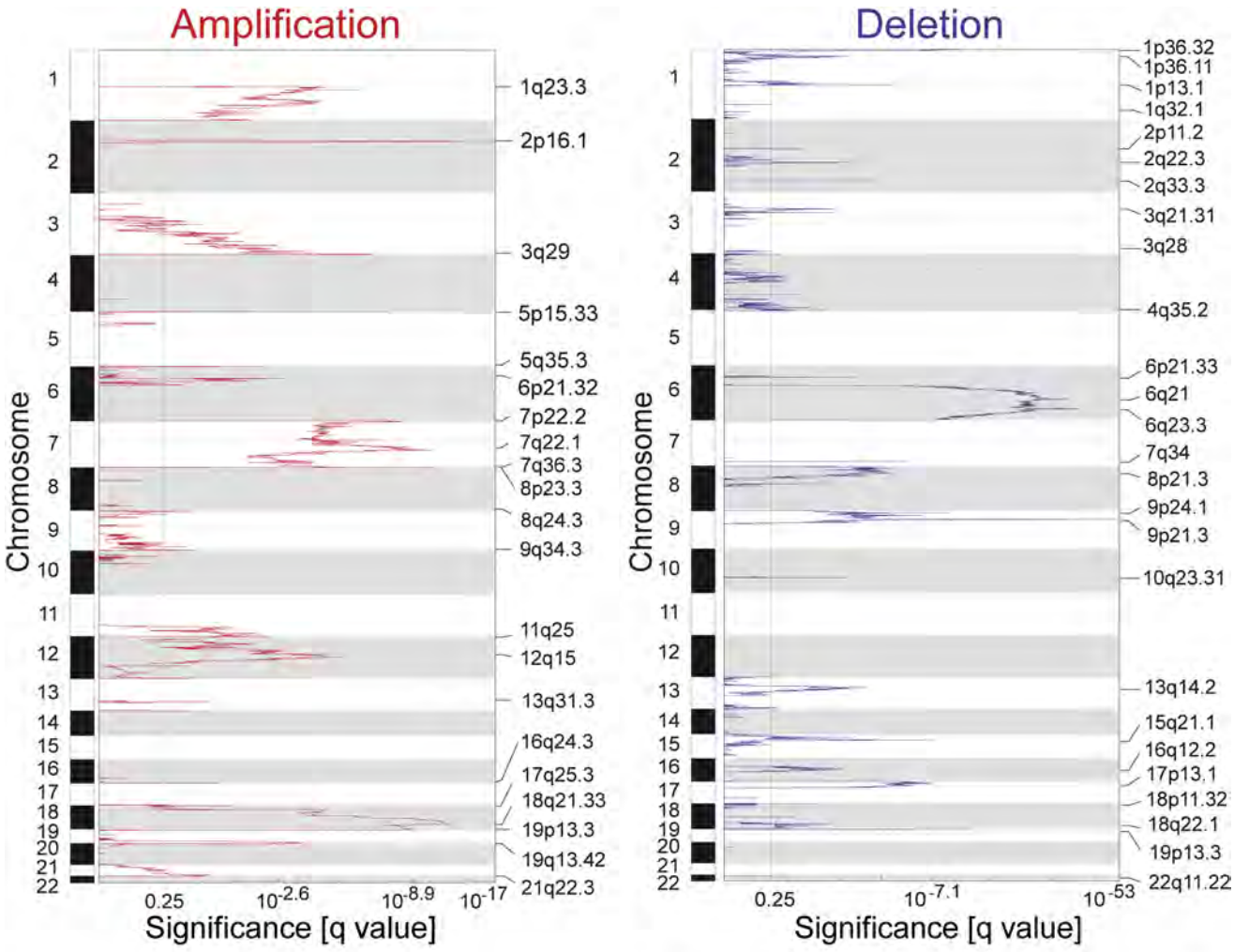

ID	Band	Peak boundaries	Top 5 genes in peak	n (%)
A1	1q23.3	chr1:159,738,009 -159,946,881	*FCRLA, FCGR2B, FCGR2C*	27 (15)
A2	2p16.1	chr2: 60,847,200 - 61,000,748	*PAPOLG, REL*	28 (16)
A3	3q29	chr3:196,744,162 - 197,538,400	*PPP1R2, PCYT1A, TFRC, APOD*	28 (16)
A4	5p15.33	chr5:1,322,366 -1,339,296		27(15)
A5	5q35.3	chr5:178,985,164 -179,067,227	*CANX*	23 (13)
A6	6p21.32	chr6: 32,798,809 - 32,867,250		21 (12)
A7	7p22.2	chr7:1-3,921,089	*HEATR2, NUDT1, UNC84A, C7ORF20, FTSJ2*	37 (21)
A8	7q22.1	chr7:100,846,670 -101,680,144		35(19)
A9	7q36.3	chr7:157,625,912 -157,638,632		37(21)
A10	8p23.3	chr8: 957,635 - 979,854	*ERICH1*	14 (8)
A11	8q24.3	chr8:144,510,826 -146,274,826	*SLC39A4, CYC1, GPR172A, RPL8, GPAA1*	19 (11)
A12	9q34.3	chr9:137,683,556 -140,273,252	*PHPT1, TUBB2C, EDF1, C9ORF86, PMPCA*	19 (11)
A13	11q25	chr11:133,857,250 -134,137,032		21(12)
A14	12q15	chr12: 67,637,703 -69,005,611	*RAB3IP, CNOT2, YEATS4, CCT2, CPSF6*	24(13
A15	13q31.3	chr13: 90,639,856 - 91,276,232		14 (8)
A16	16q24.3	chr16: 88,172,338 - 88,190,375		11 (6)
A17	17q25.3	chr17: 78,224,811-78,241,606		14 (8)
A18	18q21.33	chr18: 59,013,889 - 59,028,583	*BCL2*	33 (18)
A19	19p13.3	chr19: 211,999 - 2,134,174	*NDUFS7, RPS15, GPX4, CDC34, DAZAP1*	16 (9)
A20	19q13.42	chr19: 60,201,501- 60,985,512	*U2AF2, ISOC2, NAT14, HSPBP1, PPP1R12C*	18 (10)
A21	21q22.3	chr21: 41,771,455 - 45,917,251	*PFKL, U2AF1, ICOSLG, CSTB, PDXK*	17 (9)

ID	Band	Peak boundaries	Top 5 genes in peak	n (%)
D1	1p36.32	chr1: 2,916,416 - 3,752,748	*LRRC47, WDR8, KIAA0495*	25 (14)
D2	1p36.11	chr1: 27,103,658 - 27,413,812		16 (9)
D3	1p13.1	chr1:116,871,939 -116,913,482	*CD58*	14 (8)
D4	1q32.1	chr1: 204,650,261- 205,216,469	*RASSF5, IKBKE, IL10, PIGR*	8 (4)
D5	2p11.2	chr2: 84,971,942 - 85,173,585	*TMSB10, KCMF1*	11 (6)
D6	2q22.3	chr2:144,682,679 -145,762,089		13 (7)
D7	2q33.3	chr2: 206,441,809 - 20,6444,766		12 (7)
D8	3p21.31	chr3: 47,813,898 - 49,878,068	*DALRD3, ARIH2, UQCRC1, USP4, IHPK2*	14 (8)
D9	3q28	chr3:190,827,809 -191,035,064		9 (5)
D10	4q35.2	chr4:188,898,040 -189,271,117		13 (7)
D11	6p21.33	chr6: 31,275,478 - 31,434,938	*HLA-B, HLA-C*	12 (7)
D12	6q21	chr6:106,531,795 -106,686,165	*PRDM1*	49 (27)
D13	6q23.3	chr6:138,075,988 -138,381,526	*TNFAIP3*	44 (24)
D14	7q34	chr7:142,055,362 -142,213,197		20 (11)
D15	8p21.3	chr8:19,407,049 - 20,687,278	*INTS10, ATP6V1B2*	19 (11)
D16	9p24.1	chr9: 5,096,681 - 5,099,576	*JAK2*	23 (13)
D17	9p21.3	chr9: 21,953,431- 21,978,391	*CDKN2A*	43 (24)
D18	10q23.31	chr10: 90,587,609 - 90,765,608	*FAS, STAMBPL1, ANKRD22*	12 (7)
D19	13q14.2	chr13: 47,078,937 - 47,858,483	*MED4, RB1, NUDT15, SUCLA2, ITM2B*	16 (9)
D20	15q21.1	chr15: 42,726,553 - 42,813,414	*B2M*	19 (11)
D21	16q12.2	chr16: 52,040,758 - 52,209,001	*RBL2*	13 (7)
D22	17p13.1	chr17: 7,483,385 - 7,964,774	*TRAPPC1, CHD3, LSMD1, TP53, JMJD3*	22 (12)
D23	18p11.32	chr18:1,895,359 -1,976,213	*METTL4*	11 (6)
D24	18q22.1	chr18: 63,756,690 - 64,116,269	*TXNDC10*	14 (8)
D25	19p13.3	chr19: 6,486,980 - 6,571,909		15 (8)
D26	22q11.22	chr22: 20,835,282 - 21,596,117	*PRAME*	14 (8)

Figure 1. Recurrent CNAs in Newly Diagnosed DLBCLs

GISTIC summary plots of the significant CN gains (left panel, red) and CN losses (right panel, blue) in 180 primary DLBCLs are displayed by chromosomal position (y axis). FDR q values <.25 (right of the green line, x axis) are considered statistically significant. The chromosomal bands, GISTIC peak boundaries, frequencies of alterations (n [%]), and top five genes by integrative analyses of CN and transcript abundance are listed below.

See also Tables S1, S2, and S3.

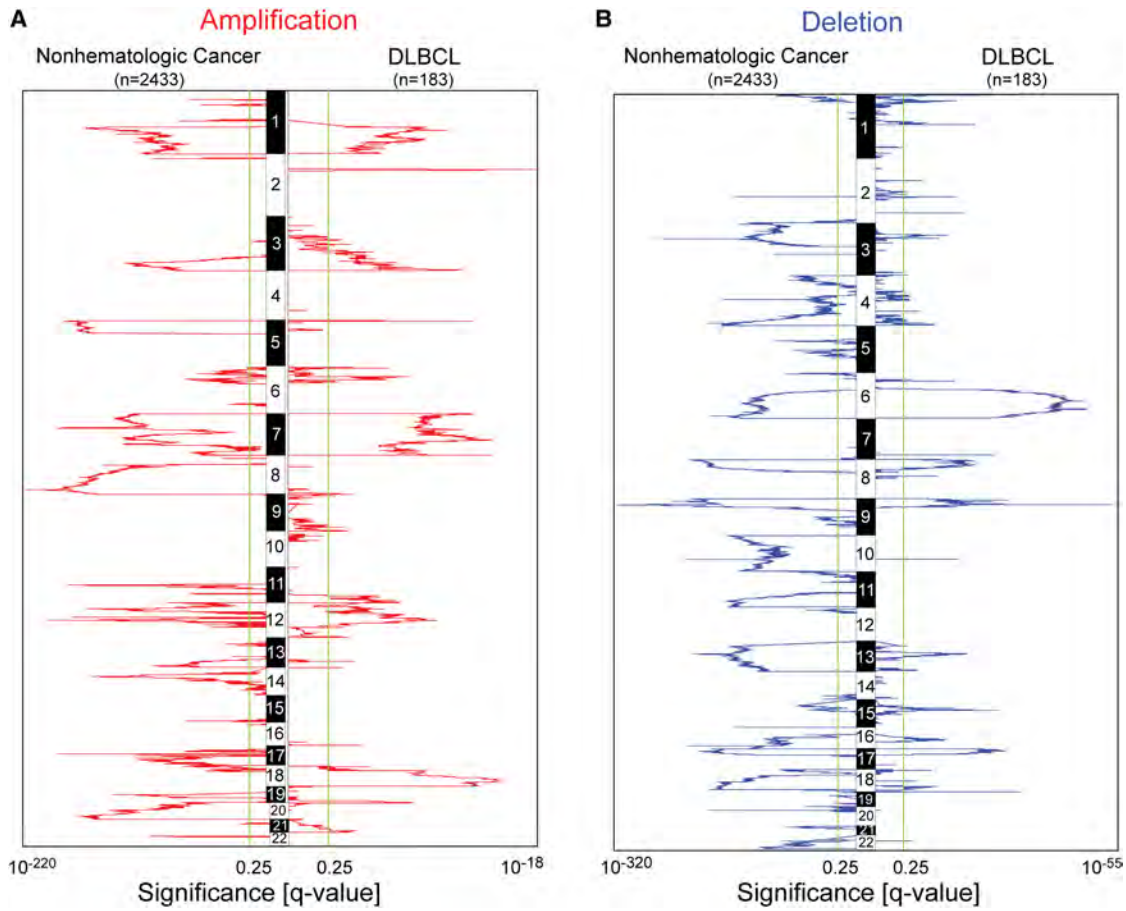

Figure 2. Comparison of CNAs in Primary DLBCLs and Nonhematologic Cancers

The GISTIC-defined recurrent CNAs in the 180 primary DLBCLs (B) are compared to those in 2,433 nonhematologic cancers from a publicly available database (A; Beroukhim et al., 2010) in a mirror plot with chromosome position on the y axis, significance (q value) on the x axis, CN gain in red and CN loss in blue. Green line denotes FDR values <.25.

See also Figure S1.

was defined as the set of within-peak (or within-region) genes with the most significant association between CN and transcript abundance (false discovery rate [FDR] q values $\leq$ .25; top five peak transcripts; Figure 1; Table S1; complete list, Table S3).

CNAs of Genes with Known Roles in Lymphomagenesis

The two genes most closely associated with the 6q21 and 6q23.3 copy loss were *PRDM1* (*BLIMP1*) and *TNFAIP3* (*A20*), respectively (Figure 1; Table S1). Both genes are confirmed tumor suppressors that can be inactivated by several mechanisms, including copy loss (Calado et al., 2010; Kato et al., 2009; Pasqualucci et al., 2006). Deletion of the ubiquitin-editing enzyme, TNFAIP3, contributes to lymphoid transformation, in part, by deregulating NFκB signaling (Shembade et al., 2010). Inactivation of the PRDM1 transcriptional repressor promotes lymphomagenesis by blocking normal plasma cell differentiation (Mandelbaum et al., 2010).

The additional tumor suppressor genes, *CDKN2A*, *RB1*, *FAS,* and *TP53* were closely associated with 9p21.3, 13q14.2, 10q23.31, and 17p13.1 copy loss, respectively (Figure 1), consistent with earlier analyses (Jardin et al., 2010; Sánchez-Beato et al., 2003). Furthermore, two well-known oncogenes were tightly linked with amplification peaks, *REL* at 2p16.1 and *BCL2* at 18q21.33 (Figure 1). Copy gains of 2p16.1/*REL* and 12q15 were more frequent in GCB DLBCLs whereas gains of 18q21.32/*BCL2* and 19q13.42 were more common in ABC tumors, as described (Table S1) (Bea et al., 2005; Lenz et al., 2008b). Given the identification of known CNAs in DLBCL, the integrative analysis will likely define additional CNAs and genes with previously unappreciated roles in the disease.

CNAs of Newly Identified Genes in DLBCL

The genes most closely associated with amplification of 1q23.3 (seen in 15% of DLBCLs) encode the low-affinity receptors for the IgG Fc receptors, *FCGR2B* (*CD32B*) and *FCGR2C*, and the related protein, *FCRLA* (*FCRL1*) (Figure 1). Increased FCGR2B expression was previously associated with adverse outcome in DLBCL (Camilleri-Broët et al., 2004), and *FCGR2C* CN variation and overexpression were linked with certain autoimmune diseases (Breunis et al., 2008). In addition, FCRLA was preferentially expressed in B cells and postulated to be an activating coreceptor (Leu et al., 2005).

Genes associated with amplification of the 19q13.42 region include protein arginine methyl tranferase 1 (*PRMT1*) and

BCL2L12 (Table S1). PRMT1 specifically dimethylates histone H4 at arginine 3, which generally serves as an activation signal (Nicholson et al., 2009). In addition, PRMT1 modifies transcription factors including FOXO1 (Yamagata et al., 2008) and signaling intermediaries such as the Igα subunit of the B cell receptor (Infantino et al., 2010). BCL2L12 is an atypical BCL2 family member with cytoplasmic and nuclear roles. Cytoplasmic BCL2L12 inhibits caspases 3 and 7, whereas nuclear BCL2L12 interacts with p53 and inhibits its binding to target gene promoters (Stegh and DePinho, 2011).

CNAs of Genes Required for Tumor Immune Recognition

In addition to identifying individual genes targeted by specific CNAs, we noted several alterations that perturbed genes required for tumor immune recognition. Copy loss of 6q21.33 decreased the abundance of the major histocompatibility complex (MHC) class I molecules, HLA-B and HLA-C, at the peak, and the MHC class I polypeptide-related sequences A and B, MICA and MICB, in the region (Figure 1; Table S1). In addition, copy loss of 15q21.1 and 1p13.1 reduced the abundance of the peak β2 microglobulin (β2M) and CD58 transcripts, respectively (Figure 1), and 19p13.3 copy loss decreased the levels of the region TNFSF9 (CD137L) transcripts (Table S1).

The β2M polypeptide associates with histocompatibility complex antigen (HLA) class I heavy chains on the cell surface to present antigen. In the absence of β2M, stable antigen-HLA class I complexes cannot be formed. Both HLA class I and *B2M* copy loss were previously described in large B cell lymphomas of immunoprivileged sites (Booman et al., 2008; Jordanova et al., 2003), and inactivating mutations and deletions of *B2M* were recently reported in DLBCLs (Challa-Malladi et al., 2011; Pasqualucci et al., 2011).

The 6q21.33 region genes, *MICA* and *MICB* (Table S1), encode ligands of the activating NKG2D receptor, which is expressed by natural killer (NK) cells and a subset of T cells (Raulet, 2003). Decreased expression of these NKG2D ligands likely limits an innate NK-cell mediated antitumor immune response.

The 1p13.1 peak gene, *CD58* (*LFA3*) (Figure 1), encodes a member of the immunoglobulin superfamily that is a ligand for the costimulatory CD2 receptor on T and NK cells. CD58 was recently reported to be the target of inactivating somatic mutations in a small subset of DLBCLs (Challa-Malladi et al., 2011; Pasqualucci et al., 2011), providing additional evidence that *CD58* loss promotes tumor immune escape.

The 19p13.3 region gene, *TNFSF9* (Table S1), encodes the ligand for the CD137 costimulatory receptor, which is expressed by follicular dendritic cells (FDC) and primed $CD8^+$ memory T cells (Middendorp et al., 2009). Interactions between TNFSF9 on GC B cells and CD137 on FDC and T cells regulate the GC B cell response, and *TNFSF9* loss promotes the development of GCB lymphomas (Middendorp et al., 2009).

Pathway Enrichment Analyses Reveal Coordinate Deregulation of p53 Signaling and Cell Cycle

After identifying CNAs of several genes required for tumor immune recognition, we sought a more comprehensive method to characterize additional pathways perturbed by CNAs in DLBCL. We first defined global *cis*-acting peak or region signatures as the union of all individual *cis*-acting peak or region signatures (Figure 3Aa). Thereafter, we performed pathway enrichment of the global signatures using a curated series of gene sets and ranked the results by FDR (Figures 3Aa and 3B, top pathways; Table S4, full analysis). In the global peak signature, 13 of 15 of the most significantly enriched gene sets reflect related aspects of p53 signaling, apoptosis, and cell cycle regulation (Figure 3B, top panel; FDR < .10). Although the gene sets have different names, they include common genes that are targeted by CNAs—*TP53*, *CDKN2A*, *RB1,* and *RBL2* (all copy loss) and *BCL2* (copy gain) (Figure 3B, top panel).

In the global region signature, the most significantly enriched gene set is the "p53 signaling pathway" (Figure 3B, bottom panel, FDR .0003). Additional p53 pathway components altered by CNAs include the p53 modifiers, *MDM2*, *MDM4*, and *RFWD2* (*COP1*) (all copy gain); p53 targets, *PERP*, *SCOTIN*, *TNFRSF10* (*DR5*/TRAIL receptor), and *FAS* (all copy loss); and critical cell cycle regulators, *CCND3* (cyclin D3), *CDK4*, *CDK6*, and *CDK2* (all copy gain) (Figure 3B, bottom panel).

Components of the p53, Apoptotic, and Cell Cycle Pathways Perturbed by CNAs

CNAs of p53, apoptotic, and cell cycle pathway members are illustrated in Figure 4.

p53 Pathway

CNAs of p53 pathway components all had the same predicted downstream effect—decreased abundance of functional p53 and reduced levels of associated p53 targets. Copy loss of *CDKN2A*, at 9p21.3, occurs in 24% of DLBCLs (Figure 4). The two alternative transcripts derived from the *CDKN2A* locus, $p16^{INK4A}$, and ARF have complementary roles in p53 signaling and cell cycle regulation. ARF interferes with binding of the MDM2 E3 ligase to p53, decreasing its ubiquitylation and proteasomal degradation (Brooks and Gu, 2006). As a consequence, *CDKNA2* deletion (ARF loss) and *MDM2* (12q15) amplification both increase the ubiquitylation and subsequent degradation of p53 (Figure 4). Two additional E3 ligases with complementary but largely nonoverlapping functions in destabilizing cellular p53 levels, MDM4 and RFWD2 (COP1), are increased by 1q23.3 copy gain (Figure 4) (Dornan et al., 2004).

Moreover, *TP53* itself and two positive p53 modifiers, *RPL26* and *KDM6B* (*JMJD3*), are targeted by 17p13.1 copy loss (Figure 4). The H3K27 demethylase, KDM6B, participates in the active removal of the repressive methyl mark from $p16^{INK4A}$-ARF, contributing to its transcriptional activation (Agger et al., 2009). Therefore, *KDM6B* copy loss represents an additional mechanism of indirectly reducing functional p53 activity (Figure 4). KDM6B also directly modulates p53 methylation, cellular distribution, and function (Sola et al., 2011). The other positive modifier of p53 activity, RPL26, binds to the 5′ untranslated region (UTR) of TP53, promotes its translation, and significantly increases stress-induced p53 levels (Chen and Kastan, 2010; Takagi et al., 2005) (Figure 4). RPL26 is also a target of MDM2, which polyubiquitylates the ribosomal protein and enhances its proteasomal degradation (Ofir-Rosenfeld et al., 2008) (Figure 4). In addition, the recently identified negative modulator of p53 transcriptional activity, *BCL2L12* (at 19q13.42), is amplified in a subset of DLBCLs (Figure 4).

Apoptotic Pathways

Independent of its role in regulating p53, *BCL2L12* amplification limits apoptosis by blocking the effector caspases 3 and 7

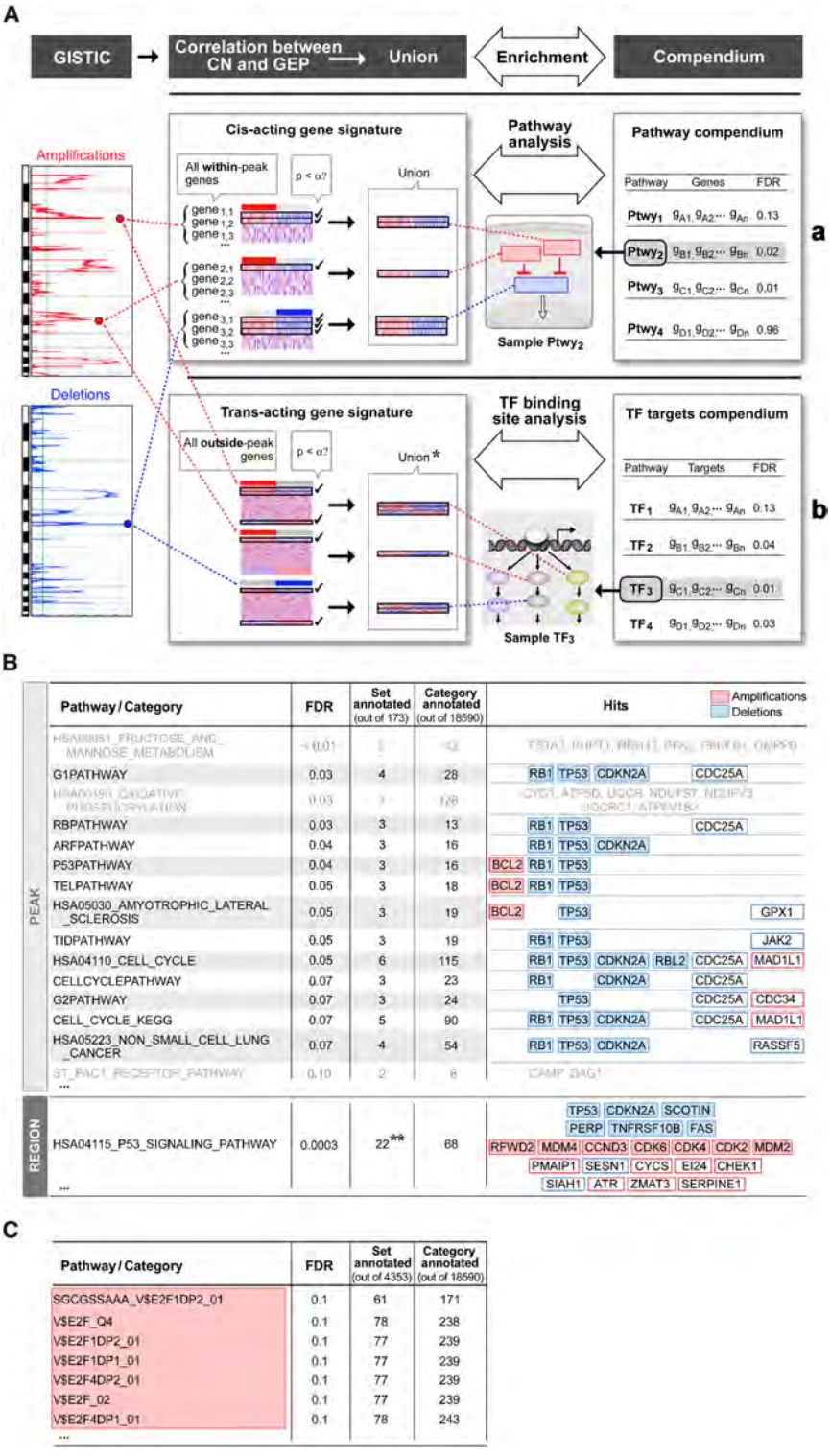

Figure 3. Pathway and TF Binding Site Enrichment

(A) Schema for pathway and TF binding site enrichment. (a) Pathway analysis. For each GISTIC peak and region, a "cis-acting gene signature" was defined, which included the genes within a GISTIC alteration with a significant (FDR <.25) correlation between CN and gene expression (left panel). The global *cis*-acting signature, the union of all individual *cis*-acting signatures, was analyzed for pathway enrichment using a pathway compendium (C2, MSigDB). (b) TF binding site analysis schema. The "trans-acting signature" of each CNA (those genes outside the CNA with the most significant association between transcript abundance and the CNA) was defined (left panel), and the union of the cis- and *trans*-acting signatures was then tested for enrichment of genes with common TF binding sites using a TF binding site compendium (C3, MSigDB).

(B) Pathway analysis. The results of global *cis*-acting signature pathway enrichment, separated for peaks (upper panel) and regions (lower panel), were ranked by FDR (FDR $\leq$ .10, peaks; top set, region; amplified genes in red, deleted genes in blue). In the region pathway analysis, the set annotation is "out of 1,893" instead of "out of 173"(**).

(C) TF binding site analysis. The results were ranked by FDR (FDR $\leq$ .1 shown here).

See also Table S4.

(Figure 4). An additional means of perturbing the intrinsic apoptotic pathway is *BCL2* copy gain (18q21.33) (Figure 4). Copy loss also decreases the abundance of several p53 targets that promote apoptosis, including the extrinsic apoptotic pathway components, *FAS*, *TNFRF10B*, *SCOTIN*, and *PERP* (Figure 4) (Beaudry et al., 2010; Bourdon et al., 2002; Wilson et al., 2009).

Cell Cycle Degregulation

The loss of $p16^{INK4A}$ and decreased abundance of p53 targets, such as p21 and GADD45, relieve repression of the cell cycle components, CCND3 (cyclin D3), CDK2, and CDK1, respectively (Figure 4). In addition, *CDK2*, *CCND3*, and the cyclin D-associated CDKs, *CDK4*, and *CDK6*, are increased by copy gain (Figure 4). In addition, *RB1* and the related RB locus, *RBL2* (p130), are targeted by copy loss in a subset of DLBCLs (Figure 4). RB1 is also a recognized target of the MDM2 E3 ligase (Polager and Ginsberg, 2009).

Signature of E2F Activation

We next sought an unbiased approach to assess the relationship between CNA-dependent changes and the abundance of E2F target genes. Because transcription factors (TF), such as E2F, will target genes outside the identified CNAs, we first defined the "trans-acting signature" of each CNA (those genes outside the CNA with the most significant association between transcript abundance and the CNA; Figure 3Ab). The union of the cis- and *trans*-acting signatures, termed the "global cis/trans-acting transcriptional signature," was then tested for

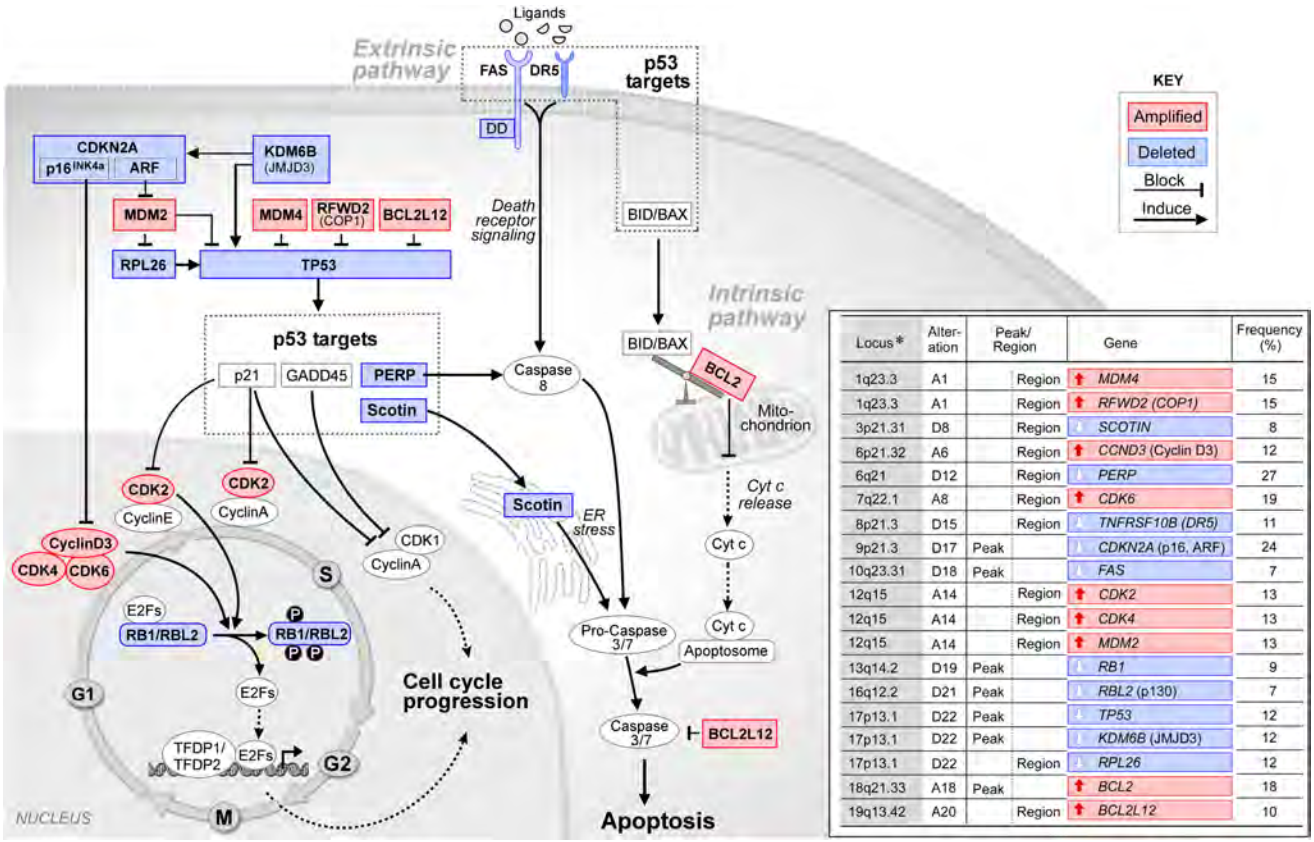

Locus*	Alter-ation	Peak/ Region	Gene	Frequency (%)
1q23.3	A1	Region	↑ *MDM4*	15
1q23.3	A1	Region	↑ *RFWD2 (COP1)*	15
3p21.31	D8	Region	↓ *SCOTIN*	8
6p21.32	A6	Region	↑ *CCND3* (Cyclin D3)	12
6q21	D12	Region	↓ *PERP*	27
7q22.1	A8	Region	↑ *CDK6*	19
8p21.3	D15	Region	↓ *TNFRSF10B (DR5)*	11
9p21.3	D17	Peak	↓ *CDKN2A* (p16, ARF)	24
10q23.31	D18	Peak	↓ *FAS*	7
12q15	A14	Region	↑ *CDK2*	13
12q15	A14	Region	↑ *CDK4*	13
12q15	A14	Region	↑ *MDM2*	13
13q14.2	D19	Peak	↓ *RB1*	9
16q12.2	D21	Peak	↓ *RBL2* (p130)	7
17p13.1	D22	Peak	↓ *TP53*	12
17p13.1	D22	Peak	↓ *KDM6B* (JMJD3)	12
17p13.1	D22	Region	↓ *RPL26*	12
18q21.33	A18	Peak	↑ *BCL2*	18
19q13.42	A20	Region	↑ *BCL2L12*	10

Figure 4. Components of the p53, Apoptotic, and Cell Cycle Pathways Perturbed by CNAs

Components include genes identified by the cis-signature pathway enrichment (Figure 3B) and three recently described p53 modifiers and cis-signature genes, *RPL26*, *KDM6B/JMJD3*, and *BCL2L12*, that are not captured by the current annotated gene sets. Amplified genes, red; deleted genes, blue. For each CNA, the locus, peak, or region gene and frequency of alteration are noted (right).

enrichment of genes with common TF binding sites (Figure 3Ab). The "global cis/trans-acting transcriptional signature" was significantly enriched for genes containing E2F binding sites; specifically, 7/7 of top-ranked binding sites were either E2F, E2F/DP1, or E2F/DP2 (Figure 3C; full list in Table S4). Therefore, DLBCL CNAs are tightly associated with cell cycle deregulation and increased abundance of E2F target genes.

Patterns of CNAs of Pathway Components

The analysis of CNAs that perturb p53 signaling, apoptosis, and cell cycle regulation also illustrates four important principles. First, a single CNA may alter several genes, which synergistically modulate the same pathway, as in 17p13.1 copy loss decreasing expression of p53 itself and the p53 modifiers, RPL26 and KDM6B (JMJD3) (Figure 4). Second, several CNAs may modify the same pathway. For example, 1q23.3 copy gain (*MDM4* and *RFWD2*), 9p21.3 copy loss (*CDKN2A*), 12q15 copy gain (*MDM2*), 17p13.1 copy loss (*TP53*, *RPL26*, and *KDM6B*), and 19q13.42 copy gain (*BCL2L12*) all function to decrease p53 activity (Figure 4). Third, certain single CNAs may alter complementary pathways, such as 12q15 amplification (*CDK2*, *CDK4*, and *MDM2*), enhancing cell cycle progression and reducing p53 activity (Figure 4). Fourth, multiple CNAs may modify complementary pathways such as p53 signaling, apoptosis, and cell cycle regulation (Figure 4).

CNAs of p53 Pathway and Cell Cycle Components in Individual Primary DLBCLs

After comprehensively defining CNAs that perturb p53 signaling and cell cycle pathways in DLBCLs, we assessed the patterns and combinations of alterations that occur in individual tumors. When the primary DLBCLs were clustered in the space of the CNAs that alter p53 pathway and cell cycle components, 66% (118/180) of tumors had multiple alterations (termed "complex") whereas the remaining 34% of tumors lacked these lesions (designated "clean"; Figure 5A). Primary DLBCLs with single copy loss of 17p13.1 (*TP53/RPL26/KDM6B*) often had CNAs perturbing an additional p53 modifier – 9p21.3 (*CDKN2A/ARF*), 19q13.42 (*BCL2L12*), 12q15 (*MDM2*), or 1q23.3 (*MDM4/RFWD2*) (Figure 5A). Of interest, CNAs of the respective p53 modifiers, *CDKN2A* (ARF, 9p21.3), *MDM2* (12q15), and *MDM4/RFWD2* (1q23.3) occurred in largely separate groups of tumors (Figure 5A). DLBCLs with CNAs of p53 pathway members frequently exhibited concurrent alterations of additional cell cycle components such as *CCND3* (6p21.32), *CDK6* (7q22.1), *CDK2/CDK4* (12q15), and/or *RB1* (13q14.2) or *RBL2* (16q12.2) (Figure 5A). Tumors with "complex" patterns of p53 pathway and cell cycle components also had more total CNAs than DLBCLs with "clean" p53/cell cycle signatures (Figure 5A, bottom panel, Σ all CNAs, "complex" versus "clean" $p < .0001$

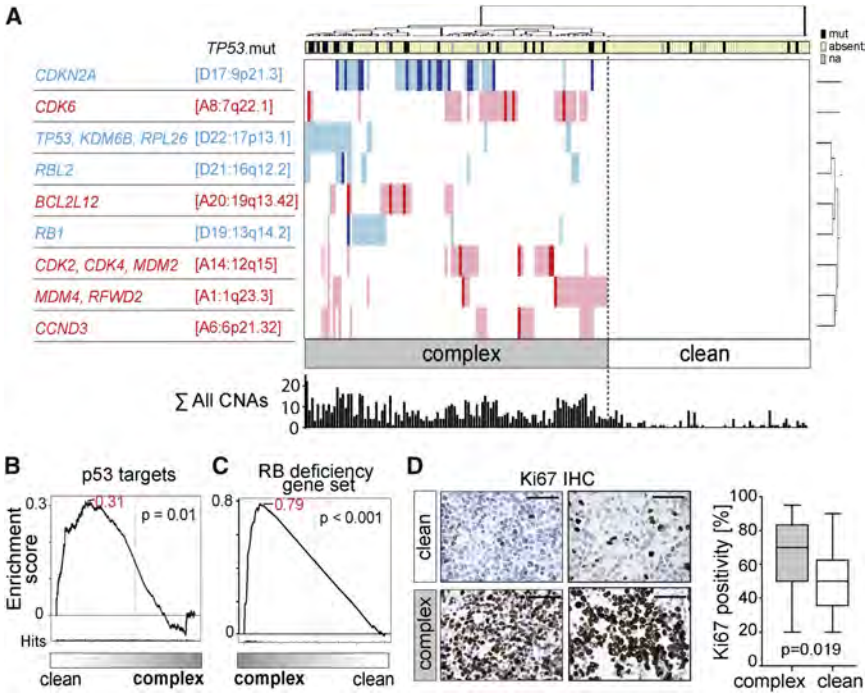

Figure 5. CNAs of p53 Pathway and Cell Cycle Components in Individual Primary DLBCLs

(A) Primary DLBCLs clustered in the space of CNAs that alter p53 pathway and cell cycle components. CNAs and perturbed genes on the left (rows) and individual tumors on top (columns). CN gains, red; CN losses, blue; color intensity corresponds to the magnitude of the CNA. Tumors with CNAs of multiple p53 pathway and cell cycle components, "complex"; DLBCLs without these lesions, "clean". Total CNAs (Σ all CNAs) in "complex" versus "clean" DLBCLs under heat map, $p < .0001$, Mann-Whitney U test. *TP53* mutations in "complex" versus "clean" DLBCLs at top, 22% versus 7%, $p < 0.005$, Fisher's one-sided exact test.

(B) GSEA of p53 targets in "clean" versus "complex" DLBCLs. The 19K genes in the genome were sorted from highest (left, white) to lowest (right, gray) relative expression in "clean" versus the "complex" DLBCLs (horizontal axis). The p53 targets (V.P53_02, described in Figure S2C) were located within the sorted genome and their positions (hits) were found to be significantly skewed toward the left end of the sorted list (positive enrichment score, 0.31), reflecting their statistically significant overexpression in "clean" as compared to "complex" DLBCLs ($p = 0.01$).

(C) GSEA of a RB deficiency gene set in "complex" versus "clean" DLBCLs. GSEA was performed as in (B) except that genes were sorted from highest to lowest expression in "complex" versus "clean" DLBCLs (horizontal axis). The positions of RB-deficiency gene set members (hits) were significantly skewed toward the left end of the sorted list reflecting their overexpression in "complex" DLBCLs (positive enrichment score 0.79, $p < 0.001$).

(D) Ki67 immunohistochemistry of "complex" and "clean" DLBCLs. Representative "clean" (upper micrographs) and "complex" DLBCLs (lower micrographs) (left). Scale bar represents 50 μm. Percentage Ki67-positive tumor cells in "complex" and "clean" DLBCLs ($p = 0.019$, Mann-Whitney U test) visualized as BoxPlot (median, line; 25% and 75% quartile, box; whiskers, minimum to maximum) (right).

See also Figure S2 and Table S5.

and Figure S2A) and more frequent *TP53* mutations (Figure 5A top panel, "complex" 22% versus "clean" 7%, $p < 0.005$; Figure S2; Table S5). The patterns of "complex" versus "clean" CNAs of p53 pathway and cell cycle components and the association between "complex" signature and total CNAs were confirmed in an independent series of 79 primary DLBCLs (Figure S2B).

To further characterize "complex" versus "clean" tumors, we performed gene set enrichment analysis (GSEA) with publicly available series of p53 target genes and a RB-deficiency gene set, which included multiple E2F targets (Knudsen and Knudsen, 2008). The GSEA computational method identifies statistically significant, concordant differences in the transcript abundance of a previously defined set of genes (such as p53 targets) in two biological states (ie, "clean" versus "complex" primary DLBCLs) (Subramanian et al., 2005). The p53 target transcripts were significantly less abundant in "complex" DLBCLs, directly linking their genetic signature of p53 deficiency with decreased p53 activity (Figures 5B and S2C). Furthermore, the RB-deficiency gene set was significantly enriched in "complex" DLBCLs suggesting that these tumors had increased E2F-mediated cell cycle progression (Figure 5C). Consistent with these observations, DLBCLs with "complex" CNA patterns also had significantly higher proliferation indices as determined by Ki67 immunostaining (Figure 5D).

Structural Complexity as a Significant Predictor of Outcome

We next assessed the prognostic significance of the "complex" CNA pattern in the subset of patients who were treated with rituxan, cyclophosphamide, adriamycin, oncovin, and prednisone (R-CHOP) and had long-term follow up (Tables S6 and S7). Patients with "complex" CNA patterns had a 5 year overall survival of only 62%, whereas those with "clean" CNA signatures were all cured (Figure 6A; $p = .001$). The association between CN complexity and outcome was independent of transcriptional COO categories (Figure S3).

We next assessed the relationship of CN complexity and the clinical IPI risk model. Although the IPI was highly predictive of outcome (low/low-intermediate versus high-intermediate/high; Figure 6B, left panel), the CNA pattern significantly increased prognostic accuracy (Figure 6B, middle and right panels). In both the low/low-intermediate and high-intermediate/high-risk groups, patients whose tumors had "complex" CNAs had significantly shorter overall survivals, whereas all patients with "clean" CNA patterns were cured (Figure 6B, middle and right panels). The contribution of the CNA pattern to IPI outcome stratification was also confirmed by a Cox-proportional hazard model ($p < .001$; Supplemental Experimental Procedures). Taken together, these data provide a structural basis for deregulated cell cycle,

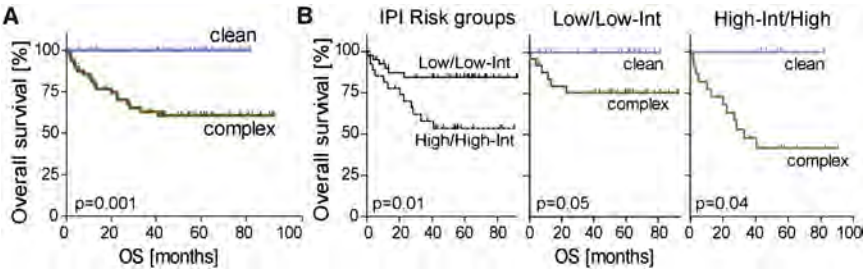

Figure 6. Prognostic Significance of "Complex" versus "Clean" CNA Pattern in DLBCLs

(A) Overall survival of R-CHOP treated DLBCL patients with "complex" versus "clean" CNA patterns (p = .001, log rank test).

(B) CNA patterns in IPI risk groups. Overall survival of R-CHOP treated DLBCL patients in low/low-intermediate and high-intermediate/high IPI risk groups (left). Overall survival of low/low-intermediate and high-intermediate/high risk patients with "complex" versus "clean" CNA patterns (middle and right).

See also Figure S3 and Tables S6 and S7.

increased cellular proliferation, and unfavorable outcome in DLBCL.

Targeting Deregulated Cell Cycle with Broad-Acting CDK Inhibitors

The predictive value of the "complex" CNA pattern and its association with deregulated cell cycle and increased activation of CDK4/6, CDK2, and likely CDK1 (Figure 4) prompted us to assess the activity of a broad-acting CDK inhibitor, such as flavopiridol (Lapenna and Giordano, 2009), in DLBCL. We used a panel of DLBCL cell lines derived from patients with relapsed/refractory disease; all lines have decreased or absent p53 activity and CNAs of cell cycle components including *CDKN2A*, *CCND3*, *CDK4*, *CDK6*, *CDK2*, and/or copy loss of *RB1* (Figure S4A). Flavopiridol, which inhibits CDK4/6, CDK2, and CDK1 (and CDK9), decreased the cellular proliferation of the DLBCL cell lines at nanomolar doses (Figure 7A). Similar results were obtained with a second pan-CDK inhibitor, AT-7519 (Figure S4B). Of interest, a DLBCL cell line with single copy *RB1* loss (DHL7), was less sensitive to lower doses of flavopiridol (Figure 7A) consistent with *RB1* being downstream of the targeted CDKs.

In these DLBCL cell lines, treatment with the pan-CDK inhibitor decreased S phase and induced cell cycle arrest (Figure 7B). In addition, the broad-acting CDK inhibitor increased apoptosis, as assessed by subG1 peaks and Annexin V/7-AAD staining (Figures 7B and 7C), and decreased the phosphorylation of RB1 at CDK4/6 and CDK2-specific sites (pS780 and pT821, respectively) (Figures 7D and S4B). In multiple DLBCL xenograft models, flavopiridol treatment significantly reduced tumor growth and lymphoma infiltration of bone marrow and spleen (Figures 8A–8C and S5). Taken together, these data suggest that genetically driven cell cycle deregulation in DLBCL may be amenable to targeted therapy.

DISCUSSION

Using a combination of high-density (HD)-SNP arrays, gene expression profiling, and pathway analyses, we have comprehensively defined CNAs, associated candidate driver genes, and perturbed signaling pathways in a large series of newly diagnosed DLBCLs. The precision of the HD-SNP platform allowed us to precisely determine the boundaries of recurrent CNAs and distinguish alterations that were unique to DLBCL from ones that were shared with nonhematologic malignancies. The multiple low frequency CNAs prompted us to systematically evaluate the alterations and associated genes with pathway analyses. The approach revealed a large complementary set of CNAs that decreased p53 activity and perturbed cell cycle regulation. The CNA-associated signature of p53 deficiency and cell cycle deregulation was highly predictive for outcome and potentially amenable to targeted therapy.

p53 Deficiency

The CNA-associated pattern of deregulated p53 signaling was detected in 66% of newly diagnosed DLBCLs, of note because somatic inactivating mutations of *TP*53 are much less common in DLBCLs than in multiple epithelial malignancies. For example, only 16% of tumors in the current series of primary DLBCLs exhibited hemizygous *TP53* mutations, and the majority of these were in "complex" tumors with additional CNAs of p53 pathway members. All of the CNAs of p53 modulators and signaling pathway components had the same functional effect—decreased abundance of functional p53 and reduced levels of p53 targets. In addition to identifying previously described CNAs of p53 modifiers, such as *CDKN2A* (ARF) and *MDM2* and *TP53* itself, we found CNAs of the p53 regulators *MDM4*, *RFWD2*, and *BCL2L12* in DLBCL. We also defined a "deletion block" on chromosome 17p13 that includes two additional p53 modifiers, *KDM6B* and *RPL26*, as well as *TP53*. The concurrent loss of *TP53*, *RPL26*, and *KDM6B* may perturb p53 signaling to a greater degree than anticipated in tumors with hemizygous 17p13 deletions. The gain of both *MDM4* and *RFWD2* at 1q23.3 delineates an additional "amplicon block" that serves to decrease p53 activity. These insights regarding genetic mechanisms that reduce normal p53 activity in DLBCL may inform targeted treatment strategies. For example, two recently developed p53 inhibitors are predicated on disrupting the interaction between functional p53 and the p53 modifiers, MDM2 and MDM4 (Bernal et al., 2010; Shangary and Wang, 2008).

Perturbed Cell Cycle Regulation

Besides copy loss of the cyclin D-dependent kinase inhibitor, $p16^{INK4A}$, we identified copy gain of *CDK4*, *CDK6*, and *CCND3*, the most abundant and essential D-type cyclin in germinal center B cells (Cato et al., 2011). In addition to the likely relief of p53/p21-dependent CDK2 inhibition, we also found copy gain of *CDK2* in association with *CDK4* (and *MDM2*) in a chromosome 12q15 "amplicon block" and copy loss of both *RB1* and *RBL2*. There was a highly significant CNA-associated signature of

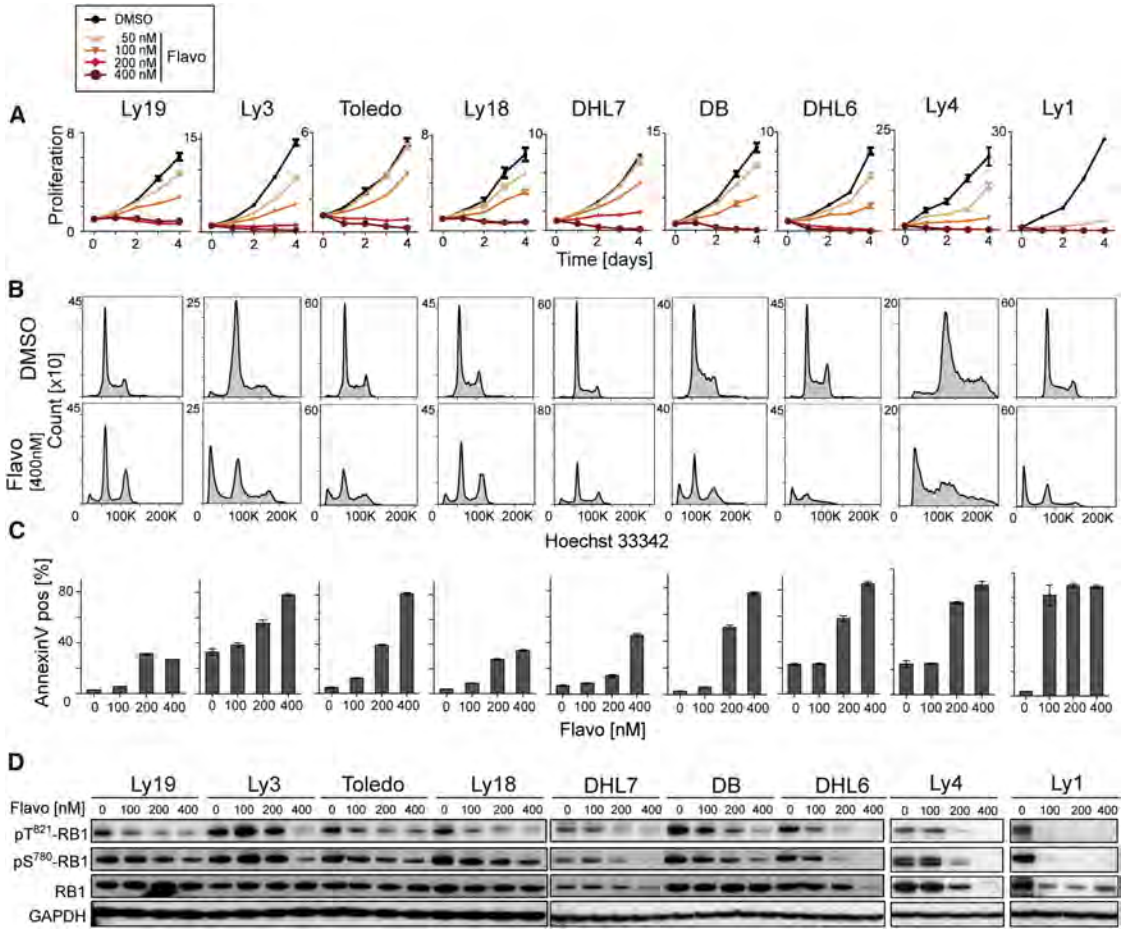

Figure 7. Targeting Deregulated Cell Cycle with a Pan-CDK Inhibitor

DLBCL cell lines with decreased or absent p53 activity and CNAs of *CDKN2A*, *CCND3*, *CDK4*, *CDK6*, *CDK2*, and/or copy loss of *RB1* were treated with the pan-CDK inhibitor, flavopiridol, which blocks CDK4/6, CDK2, and CDK1 (and CDK9).

(A) Proliferation following flavopiridol treatment (50–400 nM) for 1–4 days. DLBCL cell lines names at top.

(B) Cell cycle analysis following 72 hr flavopiridol treatment (400 nM) (DMSO control).

(C) Apoptosis (Annexin V staining) following 72 hr flavopiridol treatment (100–400 nM).

(D) RB1 phosphorylation at CDK4/6 and CDK2-specific sites (pS870 and pT821, respectively) following 24 hr flavopiridol treatment (100–400 nM). (Note that Rb is itself an E2F target; Knudsen and Knudsen, 2008.)

Error bars show the SD of triplicates. See also Figure S4.

increased E2F transcriptional activity underscoring the functional consequences of these genetic alterations.

The p53 and cell cycle component CNAs occur together in a comprehensive "complex" pattern in 66% of the primary DLBCLs; the remaining tumors have only rare CNAs. Gene set enrichment analysis revealed that DLBCLs with "complex" CNAs had significantly less abundant expression of p53 target genes, directly linking their genetic signature of p53 deficiency with decreased p53 activity. In addition, these "complex" tumors exhibited enrichment of E2F targets by GSEA and increased cellular proliferation by Ki67 immunostaining. Most importantly, the "complex" CNA pattern is highly predictive for outcome in R-CHOP treated DLBCL patients. These findings, which provide a mechanistic basis for previous observations regarding the prognostic significance of cellular proliferation in DLBCL (Broyde et al., 2009; Grogan et al., 1988; Salles et al., 2011), should be further validated in future DLBCL series.

The current study highlights the value of a comprehensive approach to identify CNA-defined alterations of p53 and cell cycle regulatory pathways, some of which have been characterized on an individual or selective basis and associated with outcome in earlier studies (Faber and Chiles, 2007; Jardin et al., 2010; Sánchez-Beato et al., 2003; Winter et al., 2010; Young et al., 2008). We find that a single CNA (17p13.1) targets several p53 modulators, multiple CNAs perturb p53 activity (1q23.3, 9p21.3, 12q15, 17p13.1, and 19q13.42) and a single CNA (12q15/*MDM2*, *CDK2*, and *CDK4*) modulates both p53 signaling and cell cycle progression. Because many of these CNAs are shared with additional nonhematologic malignancies (Figure 2), these findings may also be applicable to other tumor types. In fact, an array comparative genomic hybridization-defined "complex" pattern of copy gains and losses was recently associated with high mitotic counts and *TP53* alterations in breast cancer (reviewed in Kwei et al., 2010).

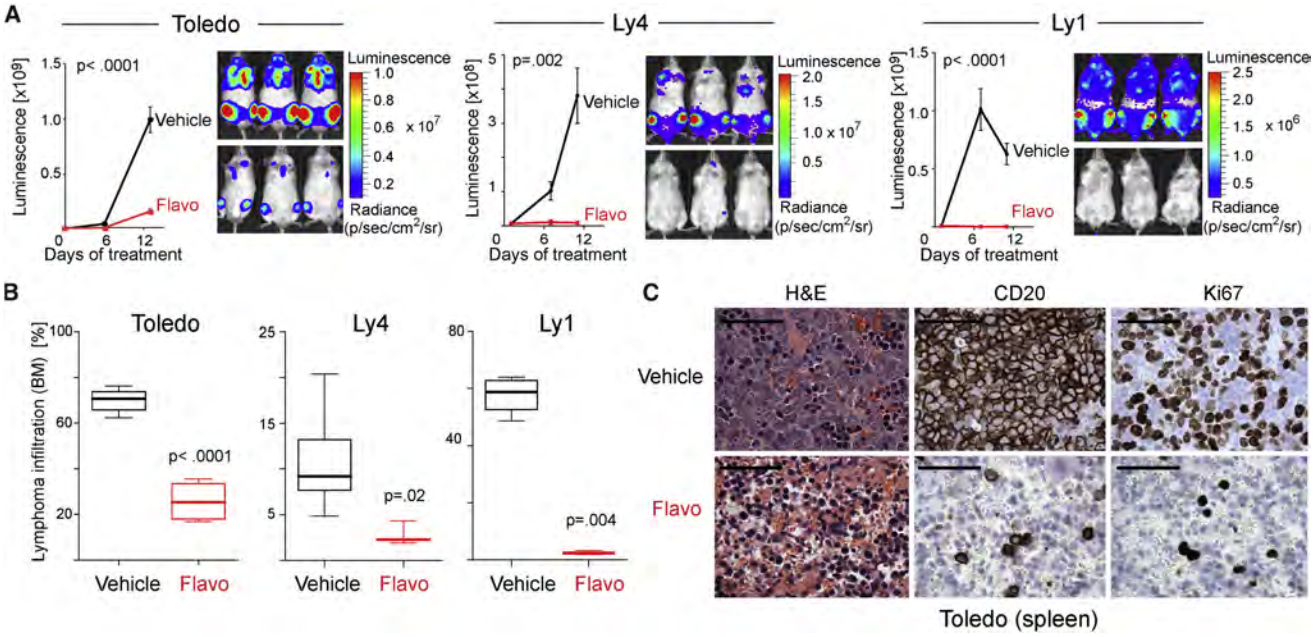

Figure 8. In Vivo Efficacy of a Pan-CDK Inhibitor in DLBCL Xenografts

(A) Bioluminescense of flavopiridol- or vehicle-treated NOD SCID Il2rγ^{null} (NSG) mice xenotransplanted with luciferized mCherry^{+} (Toledo, Ly4, or Ly1) DLBCL cells. Error bars show the SEM.

(B) Lymphoma infiltration in the bone marrow of NSG mice (in A) following flavopiridol or vehicle treatment. Single cell suspensions of bone marrow of tumor-bearing mice were evaluated for mCherry^{+} DLBCL cells by flow cytometry and visualized as Box-Plot (median, line; 25% and 75% quartile, box; whiskers, minimum to maximum). P values were obtained with a Mann-Whitney U test.

(C) Immunohistochemical analysis of lymphoma (Toledo) cell infiltration in spleens of vehicle- and flavopiridol-treated mice: H&E; anti-human CD20, and anti-Ki67 immunostaining. Scale bar represents 50 μm.

See also Figure S5.

Genomic Instability in the Subset of DLBCLs with Perturbed p53 Signaling and Cell Cycle Deregulation

In our DLBCL series, tumors with "complex" CNAs of p53 and cell cycle components also had significantly more of the additional recurrent CNAs, including focal and regional alterations and gains or losses of half or whole chromosomes (Figure S2A). The basis for the increased genomic instability in these "complex" DLBCLs remains to be defined but may be linked to the deficiencies in p53 signaling and perturbed cell cycle regulation. Numerical and structural chromosome instability (CIN) is better tolerated in a p53-deficient background and alterations of *TP53*, *MDM2*, *MDM4* (*MDMX*), the CDK2 partner, *CCNE1* (cyclin E1), and *RB1* all foster CIN (Hernando et al., 2004; Matijasevic et al., 2008; Shlien et al., 2008; Thompson et al., 2010; Wang et al., 2008). In the setting of hyperactive CDKs and DNA damage, cell cycle progression further increases genomic instability (Malumbres and Barbacid, 2009).

In addition to CNAs of the p53 apoptotic pathway, DLBCLs with the "complex" pattern exhibit alterations of other apoptotic members including *BCL2*/18q21.33, *FAS*/10q23.32, and *TNFRF10B*/8p21.3 (Figure S2A). CNAs of immune recognition molecules, including *HLA-B*, *HLA-C*, *MICA*, and *MICB* (6q21.33), *B2M* (15q21.1), *CD58*/1p13.1, and *TNFSF9* (19p13.3) also largely occur in DLBCLs with "complex" patterns (Figure S2A). These data highlight the importance of evaluating specific genetic alterations in the context of a more comprehensive assessment of CNAs and associated genomic instability.

Clinical Significance

The prognostic value of the perturbed p53 signaling/cell cycle deregulation signature prompted us to evaluate the activity of pan-CDK inhibitors in DLBCL. Following treatment, DLBCL cell lines with CNAs of p53 signaling and cell cycle components (with or without additional p53 mutations) exhibited decreased proliferation and RB1 phosphorylation and increased apoptosis in vitro and significantly reduced tumor growth in vivo. Therefore, prognostically significant, genetically driven cell cycle deregulation in DLBCL may be amenable to targeted treatment.

EXPERIMENTAL PROCEDURES

Patients and Primary Tumor Samples

High molecular weight DNA and total RNA were extracted from frozen biopsy specimens of newly diagnosed, previously untreated primary DLBCLs with ≥80% tumor involvement according to Institutional Review Board (IRB)-approved protocols from three institutions (Mayo Clinic, Brigham & Women Hospital, and Dana-Farber Cancer Institute). For one subset of patients, informed consent was obtained (Mayo Clinic). For other patients, a waiver to obtain informed consent was granted by the local IRBs because otherwise discarded tissue was used. The series included 72 DLBCLs from patients who were treated with a rituxan-containing, anthracycline-based combination chemotherapy regimen (R-CHOP-like) and had long-term follow up; 68 of these patients had available information on all clinical parameters in the IPI (Table S6).

HD-SNP Array Analysis and Expression Profiling

Primary DLBCL DNA samples and normal DNA specimens were profiled on Affymetrix HD-SNP arrays 6.0 (Supplemental Experimental Procedures). For

the detection of CN alterations, the SNP array 6.0 data was processed through a previously described analytical pipeline (Nature, 2008). Across-sample GISTIC analysis of the segmented data was carried out to identify statistically significant CNAs (Supplemental Experimental Procedures) (Beroukhim et al., 2007). Alteration regions with FDR q values below .25 were considered significant. Within each region, a peak (or peaks) was identified as the contiguous set (or sets) of loci with highest q values. To visualize the distribution of alterations across samples, we created a matrix with each entry indicating the presence/absence of an alteration (row) in a given sample (column).

RNA samples from 169 of the primary DLBCLs were transcriptionally profiled, and the data were processed using Affymetrix MAS5 summarization method (Supplemental Experimental Procedures).

Integrative Analysis

Cis-*Acting Alteration Signatures*

The genes within the peak (region) of each GISTIC-identified alteration were tested for an association between their expression (transcript abundance) and the presence/absence of the harboring alteration by a two-group t statistic with unequal variance. The *cis*-acting alteration signature for a given alteration was then defined as the set of within-peak (-region) transcripts with FDR q values $\leq$ .25.

Trans-*Acting Alteration Signatures*

The transcripts from genes, which were outside an alteration peak, were also evaluated for an association between their expression and the respective copy number alteration. The top 6,000 transcripts ranked by across-sample median absolute deviation (MAD) were used as the candidate list. The *trans*-acting alteration signature for an alteration was defined as the set of outside-peak transcripts with FDR q values $\leq$ .25 and fold change $\geq$ 1.3.

Pathway and TF Binding Site Enrichment Analysis

The global *cis*-acting signature, defined as the union of all of the individual *cis*-acting alteration signatures, was analyzed for pathway enrichment by testing the signature against curated gene sets from the MSigDB repository (C2 collection, version 2.5) (Supplemental Experimental Procedures). FDR-corrected q values were computed based on the hypergeometric distribution.

The global *trans*-acting signature was defined as the union of all *trans*-acting alteration signatures. The union of the global *cis*-acting and *trans*-acting signatures was then analyzed for enrichment of targets of specific TFs using the curated sets of TF targets in the MSigDB C3 collection (Supplemental Experimental Procedures). FDR-corrected q values were computed based on the hypergeometric distribution.

Xenograft Models

All animal studies were performed according to Dana-Farber Cancer Institute Institutional Animal Care and Use Committee-approved protocols.

ACCESSION NUMBERS

The Gene Expression Omnibus accession number for the HD-SNP 6.0 and gene expression data reported in this paper is GSE34171.

SUPPLEMENTAL INFORMATION

Supplemental Information includes seven tables, five figures, and Supplemental Experimental Procedures and can be found with this article online at http://dx.doi.org/10.1016/j.ccr.2012.07.014.

ACKNOWLEDGMENTS

This work was supported by NIH PO1CA092625. B.C. was supported by a grant from the German Research Foundation (DFG Ch 735/1-1).

Received: November 19, 2011
Revised: April 19, 2012
Accepted: July 24, 2012
Published: September 10, 2012

REFERENCES

Agger, K., Cloos, P.A.C., Rudkjaer, L., Williams, K., Andersen, G., Christensen, J., and Helin, K. (2009). The H3K27me3 demethylase JMJD3 contributes to the activation of the INK4A-ARF locus in response to oncogene- and stress-induced senescence. Genes Dev. *23*, 1171–1176.

Bea, S., Zettl, A., Wright, G., Salaverria, I., Jehn, P., Moreno, V., Burek, C., Ott, G., Puig, X., Yang, L., et al. (2005). Diffuse large B-cell lymphoma subgroups have distinct genetic profiles that influence tumor biology and improve gene-expression-based survival prediction. Blood *106*, 3183–3190.

Beaudry, V.G., Jiang, D., Dusek, R.L., Park, E.J., Knezevich, S., Ridd, K., Vogel, H., Bastian, B.C., and Attardi, L.D. (2010). Loss of the p53/p63 regulated desmosomal protein Perp promotes tumorigenesis. PLoS Genet. *6*, e1001168.

Bernal, F., Wade, M., Godes, M., Davis, T.N., Whitehead, D.G., Kung, A.L., Wahl, G.M., and Walensky, L.D. (2010). A stapled p53 helix overcomes HDMX-mediated suppression of p53. Cancer Cell *18*, 411–422.

Beroukhim, R., Getz, G., Nghiemphu, L., Barretina, J., Hsueh, T., Linhart, D., Vivanco, I., Lee, J.C., Huang, J.H., Alexander, S., et al. (2007). Assessing the significance of chromosomal aberrations in cancer: methodology and application to glioma. Proc. Natl. Acad. Sci. USA *104*, 20007–20012.

Beroukhim, R., Mermel, C.H., Porter, D., Wei, G., Raychaudhuri, S., Donovan, J., Barretina, J., Boehm, J.S., Dobson, J., Urashima, M., et al. (2010). The landscape of somatic copy-number alteration across human cancers. Nature *463*, 899–905.

Booman, M., Szuhai, K., Rosenwald, A., Hartmann, E., Kluin-Nelemans, H.C., de Jong, D., Schuuring, E., and Kluin, P.M. (2008). Genomic alterations and gene expression in primary diffuse large B-cell lymphomas of immune-privileged sites: the importance of apoptosis and immunomodulatory pathways. J. Pathol. *216*, 209–217.

Bourdon, J.-C., Renzing, J., Robertson, P.L., Fernandes, K.N., and Lane, D.P. (2002). Scotin, a novel p53-inducible proapoptotic protein located in the ER and the nuclear membrane. J. Cell Biol. *158*, 235–246.

Breunis, W.B., van Mirre, E., Bruin, M., Geissler, J., de Boer, M., Peters, M., Roos, D., de Haas, M., Koene, H.R., and Kuijpers, T.W. (2008). Copy number variation of the activating FCGR2C gene predisposes to idiopathic thrombocytopenic purpura. Blood *111*, 1029–1038.

Brooks, C.L., and Gu, W. (2006). p53 ubiquitination: Mdm2 and beyond. Mol. Cell *21*, 307–315.

Broyde, A., Boycov, O., Strenov, Y., Okon, E., Shpilberg, O., and Bairey, O. (2009). Role and prognostic significance of the Ki-67 index in non-Hodgkin's lymphoma. Am. J. Hematol. *84*, 338–343.

Calado, D.P., Zhang, B., Srinivasan, L., Sasaki, Y., Seagal, J., Unitt, C., Rodig, S., Kutok, J., Tarakhovsky, A., Schmidt-Supprian, M., and Rajewsky, K. (2010). Constitutive canonical NF-κB activation cooperates with disruption of BLIMP1 in the pathogenesis of activated B cell-like diffuse large cell lymphoma. Cancer Cell *18*, 580–589.

Camilleri-Broët, S., Cassard, L., Broët, P., Delmer, A., Le Touneau, A., Diebold, J., Fridman, W.H., Molina, T.J., and Sautès-Fridman, C. (2004). FcgammaRIIB is differentially expressed during B cell maturation and in B-cell lymphomas. Br. J. Haematol. *124*, 55–62.

Cancer Genome Atlas Research Network. (2008). Comprehensive genomic characterization defines human glioblastoma genes and core pathways. Nature *455*, 1061–1068.

Cancer Genome Atlas Research Network. (2011). Integrated genomic analyses of ovarian carcinoma. Nature *474*, 609–615.

Cato, M.H., Chintalapati, S.K., Yau, I.W., Omori, S.A., and Rickert, R.C. (2011). Cyclin D3 is selectively required for proliferative expansion of germinal center B cells. Mol. Cell. Biol. *31*, 127–137.

Challa-Malladi, M., Lieu, Y.K., Califano, O., Holmes, A.B., Bhagat, G., Murty, V.V., Dominguez-Sola, D., Pasqualucci, L., and Dalla-Favera, R. (2011). Combined genetic inactivation of β2-Microglobulin and CD58 reveals frequent escape from immune recognition in diffuse large B cell lymphoma. Cancer Cell *20*, 728–740.

Chen, J., and Kastan, M.B. (2010). 5′-3′-UTR interactions regulate p53 mRNA translation and provide a target for modulating p53 induction after DNA damage. Genes Dev. *24*, 2146–2156.

Chen, L., Monti, S., Juszczynski, P., Daley, J., Chen, W., Witzig, T.E., Habermann, T.M., Kutok, J.L., and Shipp, M.A. (2008). SYK-dependent tonic B-cell receptor signaling is a rational treatment target in diffuse large B-cell lymphoma. Blood *111*, 2230–2237.

Dornan, D., Bheddah, S., Newton, K., Ince, W., Frantz, G.D., Dowd, P., Koeppen, H., Dixit, V.M., and French, D.M. (2004). COP1, the negative regulator of p53, is overexpressed in breast and ovarian adenocarcinomas. Cancer Res. *64*, 7226–7230.

Faber, A.C., and Chiles, T.C. (2007). Inhibition of cyclin-dependent kinase-2 induces apoptosis in human diffuse large B-cell lymphomas. Cell Cycle *6*, 2982–2989.

Friedberg, J.W., and Fisher, R.I. (2008). Diffuse large B-cell lymphoma. Hematol. Oncol. Clin. North Am. *22*, 941–952, ix.

Fu, K., Weisenburger, D.D., Choi, W.W., Perry, K.D., Smith, L.M., Shi, X., Hans, C.P., Greiner, T.C., Bierman, P.J., Bociek, R.G., et al. (2008). Addition of rituximab to standard chemotherapy improves the survival of both the germinal center B-cell-like and non-germinal center B-cell-like subtypes of diffuse large B-cell lymphoma. J. Clin. Oncol. *26*, 4587–4594.

Grogan, T.M., Lippman, S.M., Spier, C.M., Slymen, D.J., Rybski, J.A., Rangel, C.S., Richter, L.C., and Miller, T.P. (1988). Independent prognostic significance of a nuclear proliferation antigen in diffuse large cell lymphomas as determined by the monoclonal antibody Ki-67. Blood *71*, 1157–1160.

Hernando, E., Nahlé, Z., Juan, G., Diaz-Rodriguez, E., Alaminos, M., Hemann, M., Michel, L., Mittal, V., Gerald, W., Benezra, R., et al. (2004). Rb inactivation promotes genomic instability by uncoupling cell cycle progression from mitotic control. Nature *430*, 797–802.

Infantino, S., Benz, B., Waldmann, T., Jung, M., Schneider, R., and Reth, M. (2010). Arginine methylation of the B cell antigen receptor promotes differentiation. J. Exp. Med. *207*, 711–719.

Jardin, F., Jais, J.-P., Molina, T.-J., Parmentier, F., Picquenot, J.-M., Ruminy, P., Tilly, H., Bastard, C., Salles, G.-A., Feugier, P., et al. (2010). Diffuse large B-cell lymphomas with CDKN2A deletion have a distinct gene expression signature and a poor prognosis under R-CHOP treatment: a GELA study. Blood *116*, 1092–1104.

Jordanova, E.S., Riemersma, S.A., Philippo, K., Schuuring, E., and Kluin, P.M. (2003). Beta2-microglobulin aberrations in diffuse large B-cell lymphoma of the testis and the central nervous system. Int. J. Cancer *103*, 393–398.

Kato, M., Sanada, M., Kato, I., Sato, Y., Takita, J., Takeuchi, K., Niwa, A., Chen, Y., Nakazaki, K., Nomoto, J., et al. (2009). Frequent inactivation of A20 in B-cell lymphomas. Nature *459*, 712–716.

Klein, U., and Dalla-Favera, R. (2008). Germinal centres: role in B-cell physiology and malignancy. Nat. Rev. Immunol. *8*, 22–33.

Knudsen, E.S., and Knudsen, K.E. (2008). Tailoring to RB: tumour suppressor status and therapeutic response. Nat. Rev. Cancer *8*, 714–724.

Kwei, K.A., Kung, Y., Salari, K., Holcomb, I.N., and Pollack, J.R. (2010). Genomic instability in breast cancer: pathogenesis and clinical implications. Mol. Oncol. *4*, 255–266.

Lapenna, S., and Giordano, A. (2009). Cell cycle kinases as therapeutic targets for cancer. Nat. Rev. Drug Discov. *8*, 547–566.

Lenz, G., and Staudt, L.M. (2010). Aggressive lymphomas. N. Engl. J. Med. *362*, 1417–1429.

Lenz, G., Wright, G., Dave, S.S., Xiao, W., Powell, J., Zhao, H., Xu, W., Tan, B., Goldschmidt, N., Iqbal, J., et al; Lymphoma/Leukemia Molecular Profiling Project. (2008a). Stromal gene signatures in large-B-cell lymphomas. N. Engl. J. Med. *359*, 2313–2323.

Lenz, G., Wright, G.W., Emre, N.C., Kohlhammer, H., Dave, S.S., Davis, R.E., Carty, S., Lam, L.T., Shaffer, A.L., Xiao, W., et al. (2008b). Molecular subtypes of diffuse large B-cell lymphoma arise by distinct genetic pathways. Proc. Natl. Acad. Sci. USA *105*, 13520–13525.

Leu, C.M., Davis, R.S., Gartland, L.A., Fine, W.D., and Cooper, M.D. (2005). FcRH1: an activation coreceptor on human B cells. Blood *105*, 1121–1126.

Lohr, J.G., Stojanov, P., Lawrence, M.S., Auclair, D., Chapuy, B., Sougnez, C., Cruz-Gordillo, P., Knoechel, B., Asmann, Y.W., Slager, S.L., et al. (2012). Discovery and prioritization of somatic mutations in diffuse large B-cell lymphoma (DLBCL) by whole-exome sequencing. Proc Natl Acad Sci USA *109*, 3879–3884.

Malumbres, M., and Barbacid, M. (2009). Cell cycle, CDKs and cancer: a changing paradigm. Nat. Rev. Cancer *9*, 153–166.

Mandelbaum, J., Bhagat, G., Tang, H., Mo, T., Brahmachary, M., Shen, Q., Chadburn, A., Rajewsky, K., Tarakhovsky, A., Pasqualucci, L., and Dalla-Favera, R. (2010). BLIMP1 is a tumor suppressor gene frequently disrupted in activated B cell-like diffuse large B cell lymphoma. Cancer Cell *18*, 568–579.

Matijasevic, Z., Krzywicka-Racka, A., Sluder, G., and Jones, S.N. (2008). MdmX regulates transformation and chromosomal stability in p53-deficient cells. Cell Cycle *7*, 2967–2973.

Middendorp, S., Xiao, Y., Song, J.Y., Peperzak, V., Krijger, P.H., Jacobs, H., and Borst, J. (2009). Mice deficient for CD137 ligand are predisposed to develop germinal center-derived B-cell lymphoma. Blood *114*, 2280–2289.

Monti, S., Savage, K.J., Kutok, J.L., Feuerhake, F., Kurtin, P., Mihm, M., Wu, B., Pasqualucci, L., Neuberg, D., Aguiar, R.C., et al. (2005). Molecular profiling of diffuse large B-cell lymphoma identifies robust subtypes including one characterized by host inflammatory response. Blood *105*, 1851–1861.

Morin, R.D., Mendez-Lago, M., Mungall, A.J., Goya, R., Mungall, K.L., Corbett, R.D., Johnson, N.A., Severson, T.M., Chiu, R., Field, M., et al. (2011). Frequent mutation of histone-modifying genes in non-Hodgkin lymphoma. Nature *476*, 298–303.

Nicholson, T.B., Chen, T., and Richard, S. (2009). The physiological and pathophysiological role of PRMT1-mediated protein arginine methylation. Pharmacol. Res. *60*, 466–474.

Ofir-Rosenfeld, Y., Boggs, K., Michael, D., Kastan, M.B., and Oren, M. (2008). Mdm2 regulates p53 mRNA translation through inhibitory interactions with ribosomal protein L26. Mol. Cell *32*, 180–189.

Pasqualucci, L., Compagno, M., Houldsworth, J., Monti, S., Grunn, A., Nandula, S.V., Aster, J.C., Murty, V.V., Shipp, M.A., and Dalla-Favera, R. (2006). Inactivation of the PRDM1/BLIMP1 gene in diffuse large B cell lymphoma. J. Exp. Med. *203*, 311–317.

Pasqualucci, L., Trifonov, V., Fabbri, G., Ma, J., Rossi, D., Chiarenza, A., Wells, V.A., Grunn, A., Messina, M., Elliot, O., et al. (2011). Analysis of the coding genome of diffuse large B-cell lymphoma. Nat. Genet. *43*, 830–837.

Polager, S., and Ginsberg, D. (2009). p53 and E2f: partners in life and death. Nat. Rev. Cancer *9*, 738–748.

Raulet, D.H. (2003). Roles of the NKG2D immunoreceptor and its ligands. Nat. Rev. Immunol. *3*, 781–790.

Salles, G., de Jong, D., Xie, W., Rosenwald, A., Chhanabhai, M., Gaulard, P., Klapper, W., Calaminici, M., Sander, B., Thorns, C., et al. (2011). Prognostic significance of immunohistochemical biomarkers in diffuse large B-cell lymphoma: a study from the Lunenburg Lymphoma Biomarker Consortium. Blood *117*, 7070–7078.

Sánchez-Beato, M., Sánchez-Aguilera, A., and Piris, M.A. (2003). Cell cycle deregulation in B-cell lymphomas. Blood *101*, 1220–1235.

Shangary, S., and Wang, S. (2008). Targeting the MDM2-p53 interaction for cancer therapy. Clin. Cancer Res. *14*, 5318–5324.

Shembade, N., Ma, A., and Harhaj, E.W. (2010). Inhibition of NF-kappaB signaling by A20 through disruption of ubiquitin enzyme complexes. Science *327*, 1135–1139.

Shipp, M., Harrington, D., Chairpersons, Anderson, J., Armitage, J., Bonadonna, G., Brittinger, G., Cabanillas, F., Canellos, G., Coiffier, B., Connors, J., et al. (1993). A predictive model for aggressive non-Hodgkin's lymphoma: The International NHL Prognostic Factors Project. N. Engl. J. Med. *329*, 987–994.

Shlien, A., Tabori, U., Marshall, C.R., Pienkowska, M., Feuk, L., Novokmet, A., Nanda, S., Druker, H., Scherer, S.W., and Malkin, D. (2008). Excessive genomic DNA copy number variation in the Li-Fraumeni cancer predisposition syndrome. Proc. Natl. Acad. Sci. USA *105*, 11264–11269.

Sola, S., Xavier, J.M., Santos, D.M., Aranha, M.M., Morgado, A.L., Jepsen, K., and Rodrigues, C.M.P. (2011). p53 interaction with JMJD3 results in its nuclear distribution during mouse neural stem cell differentiation. PLoS One *6*, e18421.

Stegh, A.H., and DePinho, R.A. (2011). Beyond effector caspase inhibition: Bcl2L12 neutralizes p53 signaling in glioblastoma. Cell Cycle *10*, 33–38.

Subramanian, A., Tamayo, P., Mootha, V.K., Mukherjee, S., Ebert, B.L., Gillette, M.A., Paulovich, A., Pomeroy, S.L., Golub, T.R., Lander, E.S., and Mesirov, J.P. (2005). Gene set enrichment analysis: a knowledge-based approach for interpreting genome-wide expression profiles. Proc. Natl. Acad. Sci. USA *102*, 15545–15550.

Takagi, M., Absalon, M.J., McLure, K.G., and Kastan, M.B. (2005). Regulation of p53 translation and induction after DNA damage by ribosomal protein L26 and nucleolin. Cell *123*, 49–63.

Thompson, S.L., Bakhoum, S.F., and Compton, D.A. (2010). Mechanisms of chromosomal instability. Curr. Biol. *20*, R285–R295.

Wang, P., Lushnikova, T., Odvody, J., Greiner, T.C., Jones, S.N., and Eischen, C.M. (2008). Elevated Mdm2 expression induces chromosomal instability and confers a survival and growth advantage to B cells. Oncogene *27*, 1590–1598.

Wilson, N.S., Dixit, V., and Ashkenazi, A. (2009). Death receptor signal transducers: nodes of coordination in immune signaling networks. Nat. Immunol. *10*, 348–355.

Winter, J.N., Li, S., Aurora, V., Variakojis, D., Nelson, B., Krajewska, M., Zhang, L., Habermann, T.M., Fisher, R.I., Macon, W.R., et al. (2010). Expression of p21 protein predicts clinical outcome in DLBCL patients older than 60 years treated with R-CHOP but not CHOP: a prospective ECOG and Southwest Oncology Group correlative study on E4494. Clin. Cancer Res. *16*, 2435–2442.

Yamagata, K., Daitoku, H., Takahashi, Y., Namiki, K., Hisatake, K., Kako, K., Mukai, H., Kasuya, Y., and Fukamizu, A. (2008). Arginine methylation of FOXO transcription factors inhibits their phosphorylation by Akt. Mol. Cell *32*, 221–231.

Young, K.H., Leroy, K., Møller, M.B., Colleoni, G.W.B., Sánchez-Beato, M., Kerbauy, F.R., Haioun, C., Eickhoff, J.C., Young, A.H., Gaulard, P., et al. (2008). Structural profiles of TP53 gene mutations predict clinical outcome in diffuse large B-cell lymphoma: an international collaborative study. Blood *112*, 3088–3098.